Л.Н. Гумилев атындағы Еуразия ұлттық университетінің ХАБАРШЫСЫ.
BULLETIN of L.N. Gumilyov Eurasian National University.
ВЕСТНИК Евразийского национального университета имени Л.Н. Гумилева.
ISSN: 2616-7034. eISSN: 2663-130X

IRSTI 34.29.25; 68.37.31; 29.31.26 https://doi.org/10.32523/2616-7034-2026-154-1-104-119
Research article

Spectral signatures of wheat rust from hyperspectral data: the potential of machine learning methods

R.M. Ualiyeva[1], A.V. Osipova[2], M.M. Kaverina*[3], S.B. Zhangazin[4], N.N. Iksat[5]

[1,2,3]Toraighyrov University, Pavlodar, Kazakhstan
[4,5]L.N. Gumilyov Eurasian National University, Astana, Kazakhstan

*E-mail: [1]ualiyeva.r@gmail.com, [2]aanastasiyaaa@internet.ru, *[3]k.ma96@mail.ru, [4]sayanzhangazin@gmail.com, [5]nurguliksat@gmail.com*

Abstract. The study presents an approach for detecting rust and differentiating lesions using hyperspectral imaging and machine learning methods. Analysis of the differences in the spectral characteristics of lesions on the wheat ear, leaf, and stem revealed patterns between light reflectance and the structure of plants and pathogens. Healthy areas have a high reflectance coefficient due to their normal cellular structure and chlorophyll content. Lower intensity was detected in desiccated areas, which is associated with moisture loss and disrupted plant structure. Areas affected by rust exhibit low reflectance coefficients, which are related to tissue degradation and the accumulation of dark pigments by the pathogens, contributing to their resistance to external stresses. This forms a distinct spectral profile, allowing for clear visual identification of the disease. As a result, with the aim of identifying the presence of lesions caused by *Puccinia graminis* and *Puccinia triticina*, a classification model based on the Random Forest algorithm was developed to recognise rust-affected zones, achieving an overall classification accuracy of 94%. The obtained values indicate the model's high potential for detecting rust lesions, confirming the promise of synergistic analysis of hyperspectral data combined with ensemble machine learning algorithms for the non-invasive detection of wheat rust diseases.
Keywords: hyperspectral imaging, spectral characteristics, plant rust, wheat agrocenosis, classification model

Introduction

Wheat rust, caused by fungi of the genus Puccinia, is a severe pathology of cereal crops. The disease causes significant damage to yield [1] and grain quality. Crop losses can reach up to 50-60% [2]. Therefore, early and accurate identification is a crucial component of phytosanitary monitoring, as even a moderate disease stage reduces the photosynthetic activity of leaves and

Received: 11.02.2026. Accepted: 13.03.2026. Available online: 31.03.2026.

**Corresponding author*

accelerates their aging, leading to deterioration in grain quality. Furthermore, different types of rust develop differently and require timely, appropriately selected control measures. Untimely detection leads to rapid expansion of disease foci and increased fungicide costs.

Hyperspectral imaging has become one of the most promising tools for disease monitoring. Using hyperspectral imaging, infected and healthy plants can be distinguished with high accuracy, enabling early detection of stripe [3-7] and leaf [5, 8, 9] rust at early stages. This technology facilitates the creation of disease recognition models that can determine the severity of infection for stripe and leaf [10, 11] rust; models based on Random Forest algorithms [12], CNN architectures, and UAV-hyperspectral data [13] show high accuracy in detecting the severity of stripe rust, while an ML model was used to recognise stem rust [14]. UAV-based hyperspectral imaging provides a reliable assessment of the spread of stem [15, 16], stripe [17-21], and leaf [21] rust in field conditions over large areas. Although multispectral imaging can identify stripe rust [22, 23], hyperspectral imaging proves to be more sensitive to the pathology compared to multispectral imaging [24] and allows for determining the stages of disease development, predicting its severity, and tracking its dynamics. In rust identification, the biophysical parameters of vegetation indices [25] and spectra [26] are important, especially narrow spectral bands in the red and near-infrared regions.

In this work, we aim to analyse the spectral characteristics of wheat samples affected by rust and to build a classification model using machine learning methods to assess the potential of hyperspectral imaging for reliable disease identification.

Materials and research methods

Spring wheat (*Triticum aestivum* L., 1753) plants affected by rust diseases caused by *Puccinia graminis* and *Puccinia triticina* were used as objects of this study (Figure 1).

We collected plant material during the 2025 growing season in the major grain-producing regions of Northeastern Kazakhstan. To obtain representative samples, plants showing rust symptoms were selected during the key phenological stages of the crop (BBCH 39-59 and 61-75), where these stages correspond to the development of the pathogens and their spread across different parts of the plant. The sampling area comprised 10 monitoring plots. Plant counts on these plots were based on 10 specimens per plot. To comprehensively cover all potential variations in symptom expression, the distance between adjacent plots ranged from 25 to 50 paces; the distance from the field edge varied between 25 and 50 meters, with further progression into the crop reaching 200-300 meters. Rectangular/triangular and diagonal (checkerboard) sampling patterns were employed to assess the spatial distribution of symptoms. Accordingly, the first pattern helped evaluate the uniformity of infection, while the second was applied for patchy or heterogeneous pathogen spread [27]. Subsequently, phytopathological diagnostics were performed on the collected samples at the Laboratory of Biological Research of Toraighyrov University (Pavlodar, Kazakhstan) in accordance with the State Standard 12044-93 "Methods for determination of disease infestation" [28].

Following this, the selected plant specimens were prepared for hyperspectral imaging. This procedure involved calibration using white and black references to convert raw sensor data into reflectance values, removal of background noise through ROI masking, and normalisation of the resulting spectral data. Hyperspectral imaging was carried out using a FigSpec FS-13 VNIR scanning camera (400-1000 nm; Hangzhou, China). The system provided 1200 spectral channels with a spectral resolution of 2.5 nm and a spatial resolution of 1920 pixels, where each

pixel size was 5.86 μm, and the frame rate was 128 frames per second using a CMOS detector [29, 30].

Figure 1. Study objects (a - wheat ear, b - wheat leaf, c - wheat stem)

The initial hyperspectral data, presented as hypercubes, were processed using Breeze software (version 2024.2.0). For spectral analysis, a PCA model and the Pixel Explore tool were applied. This allowed the use of original spectral plots to visualise spectral curves for individual plant samples across the VNIR range. Scatter plots were used to analyse pixel distribution across PCs, where colour intensity reflects point density - red indicating the highest density (PC1 representing the most pronounced spectral differences; PC2 representing spectral variability within a lesion).

To visualise the spectral channels with the greatest variance, hyperspectral cubes were projected onto two-dimensional images by creating maximum variance images. In this study, PCA served as an exploratory method to assess the spectral separability and heterogeneity of rust lesions. The Random Forest algorithm was used as a supervised classification method. The input features for each ROI consisted of spectral reflectance values across the VNIR range (400-1000 nm), as well as derived indices including mean reflectance, standard deviation, relative bandwidth, and wavelength contrast. Hyperparameter tuning was performed via mesh search, with parameters for the Random Forest set as number of trees (n estimators = 100), maximum tree depth (max depth = 10), and splitting criterion (Gini impurity). This approach was chosen to enhance model reliability and reduce the risk of overfitting, as it processes independent decision trees in parallel and aggregates their predictions to produce a final classification result [31].

Statistical analysis of the spectral data was performed using ANOVA and descriptive statistics. For each organ and tissue condition, statistical significance was assessed by calculating p-values, and effect sizes were quantified using η^2 (eta squared) and Cohen's d, emphasising organs exhibiting the most pronounced spectral differences. Model performance was evaluated using five-fold cross-validation. The 143 ROIs were selected to isolate tissue areas with lesions. To better approximate independent evaluation and reduce potential bias, the ROIs were split plant-wise, so that ROIs from the same plant did not appear in both the training and validation folds. In each iteration of the five-fold cross-validation, approximately 70% of the ROIs were used for training, and 30% for validation, and performance metrics (F1-score, Precision, Recall) were averaged across all folds to assess internal stability. The approach used reduces the likelihood of overfitting and allows for a reliable evaluation of the model.

Results

The figures present hyperspectral images of wheat ear, leaf, and stem affected by rust, accompanied by the Raw Spectrum graphs showing curves that reflect the spectral characteristics of plant areas, and a Variance Scatter diagram. The hyperspectral image is characterised by being coloured in conditional colours that correspond to the level of light reflectance intensity. Here, warm colours (red, yellow) denote areas with high reflectance, while cold colours (light blue, blue) indicate zones of low reflectance. The Raw Spectrum graph contains curves reflecting the spectral characteristics of specific regions of the hyperspectral image. On the other hand, the Variance Scatter diagram represents the distribution of spectral data after dimensionality reduction, where each point corresponds to a single pixel of the hyperspectral image, which is transformed into principal component coordinates. Considering the object localisation in the image, it can be noted that the colours of the areas corresponding to the curves of different colours are indicated on its right side: for example, the red curve corresponds to the blue colour on the hyperspectral image, as follows from the colour scale.

Figure 2 depicts an ear affected by the rust pathogen. It is worth noting that the red curve corresponds to the rust-affected area of the ear at its base with a reflectance of 23%. The remaining curves belong to healthy areas of the ear, where the reflectance varies within 15-30%. The spectral peaks belonging to the ear were in the wavelength range of 550-780 nm, which is standard for all examined samples. Notably, this range includes the red edge region, known for its sensitivity to the physiological state of plants. In the Variance Scatter, the first component t[1] (73.2%) reflects the majority of data variation and differences between spectra, while the second component t[2] (6.15%) shows additional variations. The high t[1] values within the explained variance indicate the dominance of spectral values characteristic of healthy ear areas, whereas t[2] primarily explains spectral deviations associated with local lesion areas. Overall, the points were grouped into one cluster, indicating that a large number of pixels have similar spectral characteristics. The presence of individual outliers is represented by the image of rare points, which reflect rust areas with distinct spectral properties, confirming the possibility of identifying regions with altered optical characteristics (Figure 2).

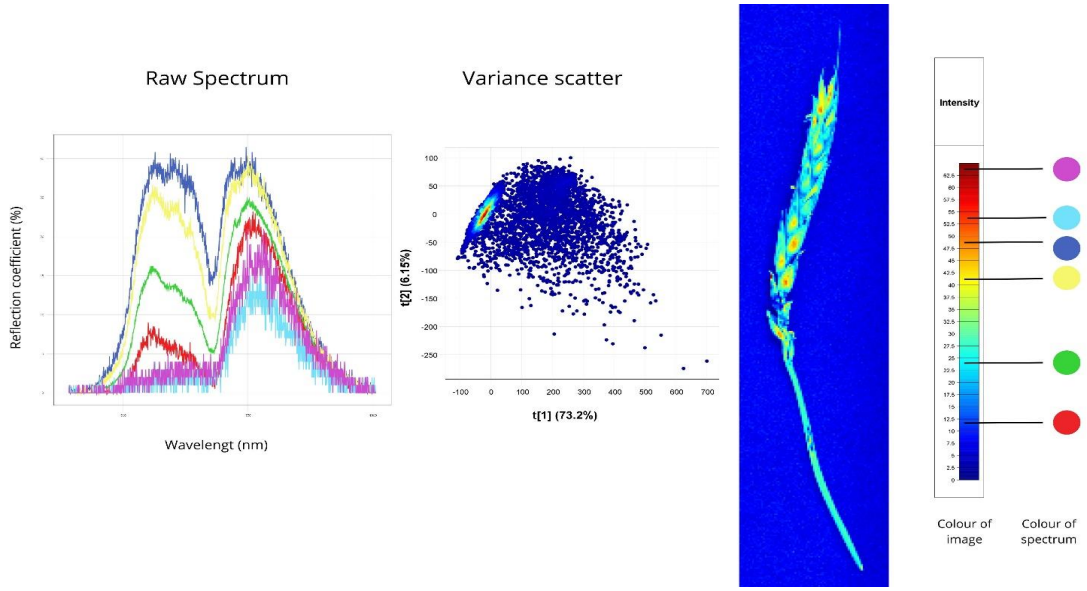

Figure 2. Spectral characteristics of a wheat ear affected by rust

Figure 3 depicts a rust-affected leaf, where the red curve reflects individual rust foci with an average reflectance of 15%. Here, the yellow curve describes areas surrounding the disease foci with a reflectance identical to the previous one - 15%. The similarity of spectra inherent to the infection foci may predominantly indicate that the disease was characterised by the onset of infection symptom development, or it may point to underlying physiological changes that were relatively difficult to distinguish visually. The purple curve belongs to desiccated areas of the leaf, where reflectance values of 25% were noted, which, in most cases, is explained precisely by the degradation of cellular structure and disruption of water balance. Alongside this, the remaining curves correspond to healthy tissue and have a reflectance in the range of 20-35%, the primary reason for which may be the relative variability of lighting conditions and the anatomical heterogeneity of the foliar organ's structure. It is important to note that the maximum spectral peaks were in the 550-780 nm range, corresponding to the region sensitive to stress impacts. The Variance Scatter diagram is characterised by an elongated shape, where the actual percentage of scattered points, reflecting pixels differing in spectral properties, is 4.56%, indicating a relative predominance of homogeneous spectral characteristics with locally pronounced areas of deviations (lesions by the rust pathogen) (Figure 3).

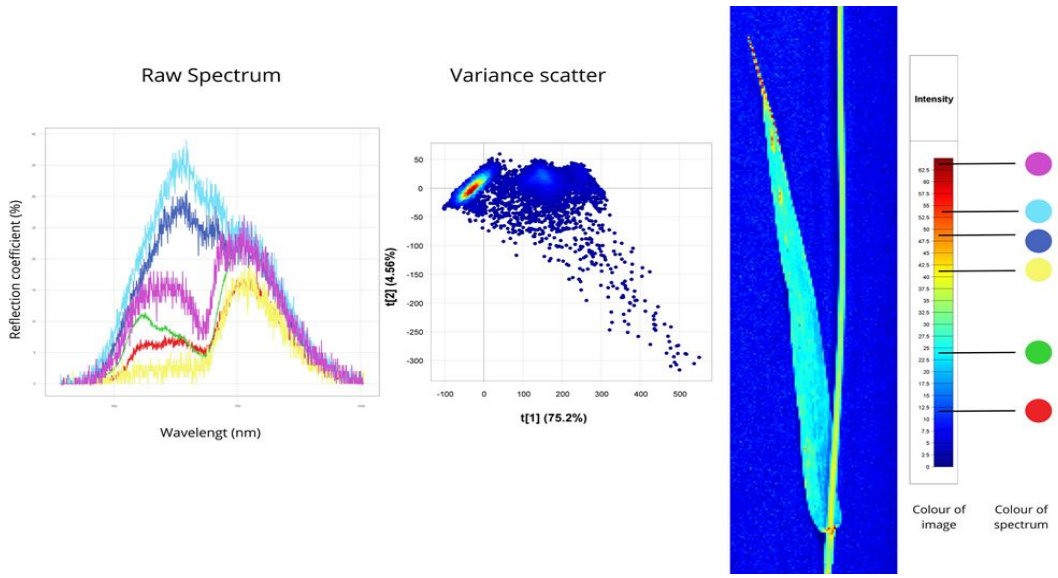

Figure 3. Spectral characteristics of a wheat leaf affected by rust

Colour differences between various areas of the stem essentially indicate a disruption of physiological processes or may be a result of tissue degradation. Figure 4 depicts a diseased stem, where the red and green curves belong to diseased areas; here, the red reflects the most severely affected areas with a reflectance of 8%, while the green curve has a reflectance within 15%. These low values may be associated with the accumulation of pathogenic biomass or the destruction of cell structure. The yellow curve corresponds to desiccated areas of the stem (28%), whereas the remaining curves represent regions retaining a healthy green colour (30-35%), primarily due to the preservation of pigments and lower moisture content. The wavelength range of the spectral peaks, as with other areas, was noted within 550-780 nm, which is a result of the physiological sensitivity of plant tissues to pathological impacts. The Variance Scatter contains numerous points, accounting for 6.24%, reflecting the heterogeneity of the stem surface due to the spectral features of disease lesions.

A comparative analysis conducted on the spectral profiles of different plant organs enables the investigation of optical properties of individual areas depending on the physiological state and anatomical structure of the studied samples. Figure 5 demonstrates the spectral profiles of different parts of wheat: ear, leaf, and stem. It has been established that the red curve reflects the spectral characteristics of the ear with a reflectance of 11-18%, the green curve belongs to the leaf and has a reflectance of 10-21%, while the blue curve describes the stem, where reflectance was within 14-21%. These differences were primarily determined by chlorophyll content, structural features of tissues, and an indicator such as moisture content. The identified spectral indicators were determined within the 550-780 nm range, which primarily correspond to regions of maximum sensitivity. This fact is associated with various pathological changes occurring in the tissues of plant organisms and is used as an informative identifier for differentiating lesions.

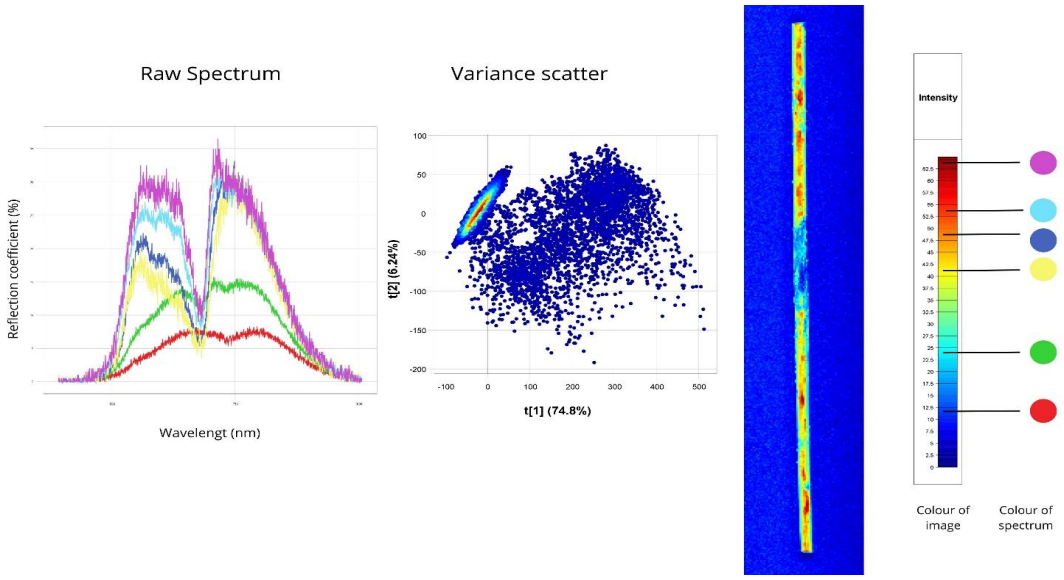

Figure 4. Spectral characteristics of a wheat stem affected by rust

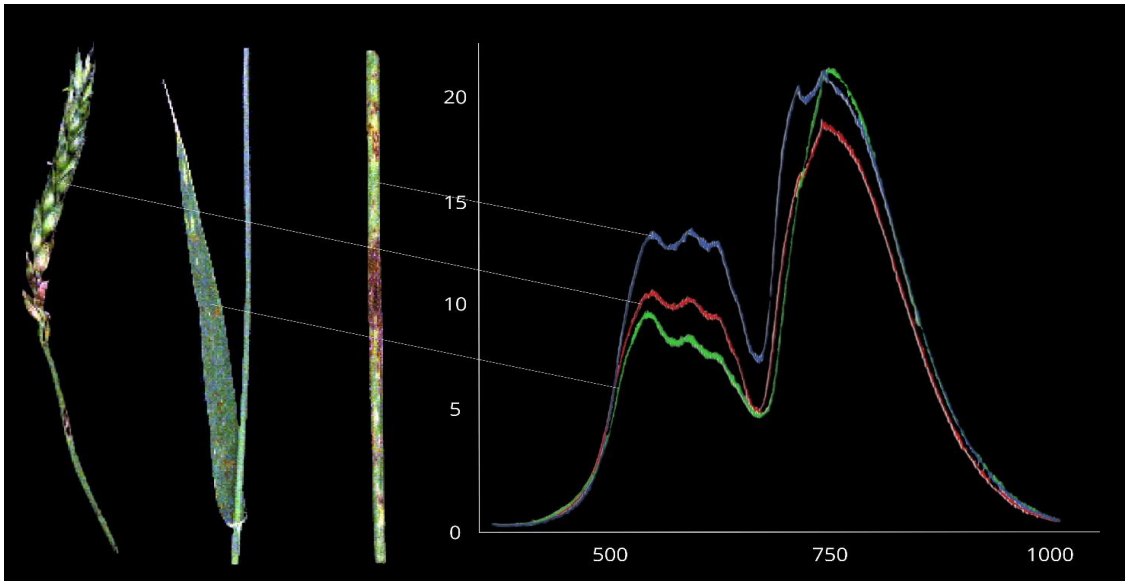

Figure 5. Comparative spectral profiles of wheat ear, leaf, and stem

Descriptive statistical indicators and the results of the analysis of variance for the reflectance and wavelength range are presented in Tables 1 and 2, respectively. The data in Table 1 show quite pronounced indicators of the reflectance associated with different functional states. It should be noted that, in several cases, the statistical analysis yielded a standard deviation of zero. This result arises because the calculations were based on the reflectance coefficient, which exhibited a single pronounced peak. Under these conditions, the absence of variability in the parameter leads to a zero-standard deviation. Therefore, in the present case, the magnitude of the standard deviation is determined not by the distribution of values across the entire spectral range, but by the presence and number of pronounced peaks in the spectrum. Spectra containing two or more distinct peaks exhibited non-zero variance, reflecting differences in their amplitude characteristics. The average value of the coefficient for the affected areas was approximately 23%, while for the entire sample as a whole, it was only 14.5%, which is 60% lower than the first indicator. Healthy ear areas are characterized by a wide wavelength range, which accompanies increased variability indicators (CV=8.47%) and indicates the actual heterogeneity of the optical properties of undamaged tissue.

Desiccated leaf areas have an average reflectance (25-28%) distinguished by its stability, which corresponds to reduced moisture content, as well as degradation of tissue structure, and is confirmed by zero values of standard deviation and variation indicators. The stem exhibits more pronounced differentiation of spectral characteristics. Differences in reflectance indicators are manifested precisely in the fact that affected areas exhibit minimal reflectance values, whereas healthy areas show maximum values (11.5% and 32.5%, respectively). Moreover, the main reflectance difference (Δ) with the maximum value was recorded within 10.58%, which corresponds to a healthy leaf and ear, and is a result of the sensitivity of this parameter, reflecting primarily the physiological state of the plants.

Table 1

Spectral characteristics of wheat samples: Reflectance

№	Plant part	Body part	Reflectance (coefficient) (%)	Mean Reflectance, Median	Standard Deviation	CV	Rate of Chan ge	Δ Reflec tance
1	Ear	Body	11-18	14.5	0.89	6.13	14.50	4.94
		Affected areas	23	23.0	0.00	0.00	23.00	0.00
		Healthy areas	15-30	22.5	1.91	8.47	22.50	10.58
2	Leaf	Body	10-21	15.5	1.40	9.01	15.50	7.76
		Affected areas	15	15.0	0.00	0.00	15.00	0.00
		Dried areas	25	25.0	0.00	0.00	25.00	0.00
		Healthy areas	20-35	27.5	1.91	6.93	27.50	10.58
3	Stem	Body	14-21	17.5	0.89	5.08	17.50	4.94
		Affected areas	8-15	11.5	0.89	7.73	11.50	4.94
		Dried areas	28	28.0	0.00	0.00	28.00	0.00
		Healthy areas	30-35	32.5	0.64	1.95	32.50	3.53

The results presented in Table 2 demonstrate that, regardless of the condition of the plant tissue or organ, all main spectral characteristics were noted in the wavelength range of 550-780 nm. Thus, the following indicators were obtained: constancy of the spectral range width within 230 nm, contrast ratio of 1.42, relative bandwidth - 0.173, and normalized contrast - 0.295.

This indicates that the key differences between the samples were related to changes in light reflectance rather than to shifts in spectral range width or peaks.

Table 2

Spectral characteristics of wheat: Wavelength

№	Plant part	Wavelength (nm)	Spectral Bandwidth	Contrast ratio	Relative bandwidth	Normalised contrast
1	Ear	550-780	230	1.42	0.173	0.295
2	Leaf	550-780	230	1.42	0.173	0.295
3	Stem	550-780	230	1.42	0.173	0.295

These observations were confirmed by statistical analysis (Table 3). The factor studied had a highly significant effect on stem and leaf reflectance ($p<0.001$) with large effect sizes ($\eta^2=0.41$ and 0.38; Cohen's d=1.25 and 1.10, respectively), reflecting the fact that rust pathogens predominantly affect leaves and stems. In contrast, the effect on ear reflectance was not statistically significant ($p=0.16$) and corresponded to a small effect size ($\eta^2=0.02$; Cohen's d=0.18). These results indicate that stem and leaf reflectance are the most informative parameters for differentiating tissue conditions, confirming their utility as indicators in diagnosing phytopathological conditions of wheat.

Overall, it was found that the most informative among the statistical data were the reflectance indicators, which allow for more accurate differentiation of desiccated, affected, and healthy tissue areas on plant samples, confirming their expediency for use as indicators in diagnosing phytopathological conditions of wheat.

After processing the spectral data, categories were added for different zones of the hyperspectral images of wheat parts. Figure 6 shows key information about the classification model built using the Random Forest machine learning algorithm. The core of the Random Forest method in this context involves generating many independent decision variants and then aggregating their outputs; this is, done by creating random samples from the original data, each used to train an individual decision tree. The results from all these trees are then averaged to produce the final rust classification model with high accuracy.

Table 3

Spectral characteristics of wheat: Wavelength

№	Plant part	p-value	η^2	Cohen's d
1	Ear	0.16	0.02	0.18
2	Leaf	<0.001	0.38	1.10
3	Stem	<0.001	0.41	1.25

The statistical data of the algorithm are presented under the letter D. Macro Accuracy, equal to 0.74074, indicates a fairly good balanced accuracy across all examined classes. Micro Accuracy shows the proportion of all correctly classified zones and is about 89%. Log loss is less than 0.3, which is a sign of a stable model and indicates a low probability error, and Log Loss Reduction within 0.69 is an indicator of the model's quality improvement compared to the baseline. The cross-validation value confirms model stability when applied to various subsamples, but at the same time it may indicate potential for further improvement by retraining on additional data.

The confusion matrix (C) presents classification performance metrics such as Recall, Precision, and the F1-score. Precision shows how accurate the model's predictions are and ranges from 92.9% to 97.6%; Recall, meanwhile, reflects how well the model finds all diseased areas, and as a result, ranges from 86.7% to 100%. The F1-score is the harmonic mean between Precision and Recall and shows how balanced the model is, where experimentally obtained data were noted within the range of 89.7% to 96.5%. Thus, rust-affected leaf areas were classified with the highest accuracy (100%), good classification performance was observed for stem zones (95.4%), whereas only 86.7% of leaf zones were correctly classified. In Figure 6, under letters A and B, the area parameter is visible, which shows the size of the affected areas, allowing for a visual comparison of the scale of the lesions.

Discussion

Rust pathogens are obligate fungi of the genus *Puccinia.* Brown leaf rust is caused by *P. triticina,* black stem rust by *P. graminis f. sp. tritici,* and yellow stripe rust by P. *striiformis f. sp. tritici* [32]. Their spores land on the plant, penetrate tissues via haustoria, and as a result, secrete effector proteins that suppress plant immunity [33, 34].

Sa... /	Group	Image	Category	Random Forest	Random Forest	Area
12.5.6. ...	Group		Stem rust		Stem rust	776 px
12.5.6. ...	Group		Stem rust		Stem rust	480 px
12.5.6. ...	Group		Stem rust		Stem rust	799 px
12.5.6. ...	Group		Stem rust		Stem rust	873 px
12.5.6. ...	Group		Stem rust		Stem rust	873 px
12.5.6. ...	Group		Stem rust		Stem rust	555 px
12.5.6. ...	Group		Stem rust		Stem rust	33 px
12.5.6. ...	Group		Stem rust		Stem rust	242 px
12.5.6. ...	Group		Stem rust		Stem rust	45 px
12.5.6. ...	Group		Stem rust		Stem rust	733 px
12.5.6. ...	Group		Stem rust		Stem rust	776 px
12.5.6. ...	Group		Stem rust		Stem rust	776 px
12.5.6. ...	Group		Stem rust		Stem rust	728 px
12.5.6. ...	Group		Stem rust		Stem rust	585 px
12.5.6. ...	Group		Stem rust		Stem rust	482 px
12.5.6. ...	Group		Stem rust		Stem rust	344 px
12.5.6. ...	Group		Stem rust		Stem rust	528 px
12.5.6. ...	Group		Stem rust		Stem rust	798 px
12.5.6. ...	Group		Stem rust		Stem rust	689 px
7.1.2. П...	Group		Ear rust		Ear rust	144 px
7.1.2. П...	Group		Ear rust		Ear rust	144 px
7.1.2. П...	Group		Ear rust		Ear rust	144 px
7.1.2. П...	Group		Ear rust		Ear rust	72 px
7.1.2. П...	Group		Ear rust		Ear rust	48 px
7.1.2. П...	Group		Ear rust		Ear rust	108 px
7.1.2. П...	Group		Ear rust		Ear rust	8 px
7.1.2. П...	Group		Ear rust		Ear rust	8 px
7.1.2. П...	Group		Ear rust		Ear rust	8 px
7.1.2. П...	Group		Ear rust		Ear rust	8 px
7.1.2. П...	Group		Ear rust		Ear rust	8 px
7.1.2. П...	Group		Ear rust		Ear rust	36 px
7.1.2. П...	Group		Ear rust		Ear rust	137 px

7.1.2. П...	Group		Ear rust		Ear rust	275 px
7.1.2. П...	Group		Ear rust		Ear rust	208 px
7.1.2. П...	Group		Ear rust		Ear rust	226 px
7.1.2. П...	Group		Ear rust		Ear rust	60 px
7.1.2. П...	Group		Ear rust		Ear rust	12 px
7.1.2. П...	Group		Ear rust		Ear rust	12 px
8.1.2. П...	Group		Leaf rust		Leaf rust	8 px
8.1.2. П...	Group		Leaf rust		Leaf rust	8 px
8.1.2. П...	Group		Leaf rust		Leaf rust	8 px
8.1.2. П...	Group		Leaf rust		Leaf rust	8 px
8.1.2. П...	Group		Leaf rust		Leaf rust	8 px
8.1.2. П...	Group		Leaf rust		Leaf rust	8 px
8.1.2. П...	Group		Leaf rust		Leaf rust	8 px
8.1.2. П...	Group		Leaf rust		Leaf rust	2 px
8.1.2. П...	Group		Leaf rust		Leaf rust	2 px
8.1.2. П...	Group		Leaf rust		Leaf rust	2 px
8.1.2. П...	Group		Leaf rust		Leaf rust	2 px
8.1.2. П...	Group		Leaf rust		Leaf rust	2 px
8.1.2. П...	Group		Leaf rust		Leaf rust	2 px
8.1.2. П...	Group		Leaf rust		Leaf rust	2 px
8.1.2. П...	Group		Leaf rust		Leaf rust	2 px
8.1.2. П...	Group		Leaf rust		Leaf rust	2 px
8.1.2. П...	Group		Leaf rust		Leaf rust	2 px
8.1.2. П...	Group		Leaf rust		Leaf rust	2 px
8.1.2. П...	Group		Leaf rust		Leaf rust	2 px

A

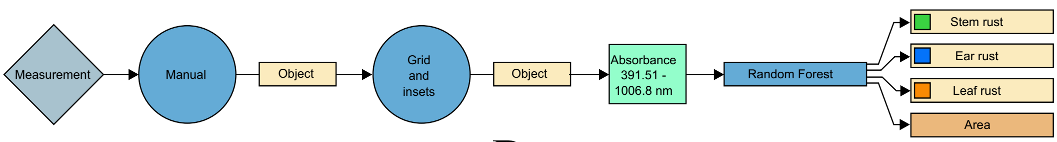

B

Actual classes	Total	Stem rust	Ear rust	Leaf rust	No class
Stem rust	87 (60.8%)	83 (95.4%)	1 (1.15%)	3 (3.45%)	
Ear rust	15 (10.5%)	2 (13.3%)	13 (86.7%)		
Leaf rust	41 (28.7%)			41 (100%)	
# Predicted	143 (100%)	85 (59.4%)	14 (9.79%)	44 (30.8%)	0
Correctly	137 (95.8%)				
Incorrectly	6 (4.2%)				
Precision		97.6%	92.9%	93.2%	
Reca		95.4%	86.7%	100%	
F-score		96.5%	89.7%	96.5%	

C

Algorithm Name	Macro Accuracy	Log Loss	Log Loss Reduction	Micro Accuracy	Cross Validation ...
Random Forest (Fast..	0.74074	0.28815	0.68811	0.89286	0.64829

D

Figure 6. Classification model (A - selected zones, B - analyse tree, C - confusion matrix, D - model statistics)

Our experimental data confirm that healthy areas have greater reflectance intensity compared to affected and desiccated ones, with the rust-affected areas having the lowest reflectance values. It is also important to note that among all plant parts, the ear possesses the lowest reflectance intensity, although the actual difference between the reflectances is practically insignificant.

Figure 7 shows the dependence between pigment content and the degree of light reflectance. As follows from the figure, red arrows indicate the degree of actual light reflectance. Thus, healthy plant tissue has a high reflectance, which is due to the green pigment chlorophyll, reflecting light in the green range of the visible spectrum (500-600 nm) and in the near-infrared range (from 700 nm). Furthermore, it has been established that the decrease in reflectance intensity of affected areas is primarily associated with the dark pigmentation of the disease. Equally important is the fact that rust pathogens contain DHN-melanins [35], for example, in black stem rust, and carotenoids (phytoene, lycopene, γ-carotene, and β-carotene), for example, in yellow stripe rust [36]. These are primarily used to provide direct protection for the pathogen against ultraviolet light, as well as to shield it from oxidative stress.

Our analysis also revealed that different types of rust can exhibit varied spectral indicators, which may depend on pigment content. The main reasons for this may be disruption of the epidermis structure, the presence of the pathogen's dark pigment, destruction of the mesophyll, and inhibition of chlorophyll synthesis, which consequently leads to reduced light reflectance in diseased areas and the plant as a whole. Accordingly, the decrease in reflectance is one of the key diagnostic indicators for rust identification in direct spectral analysis.

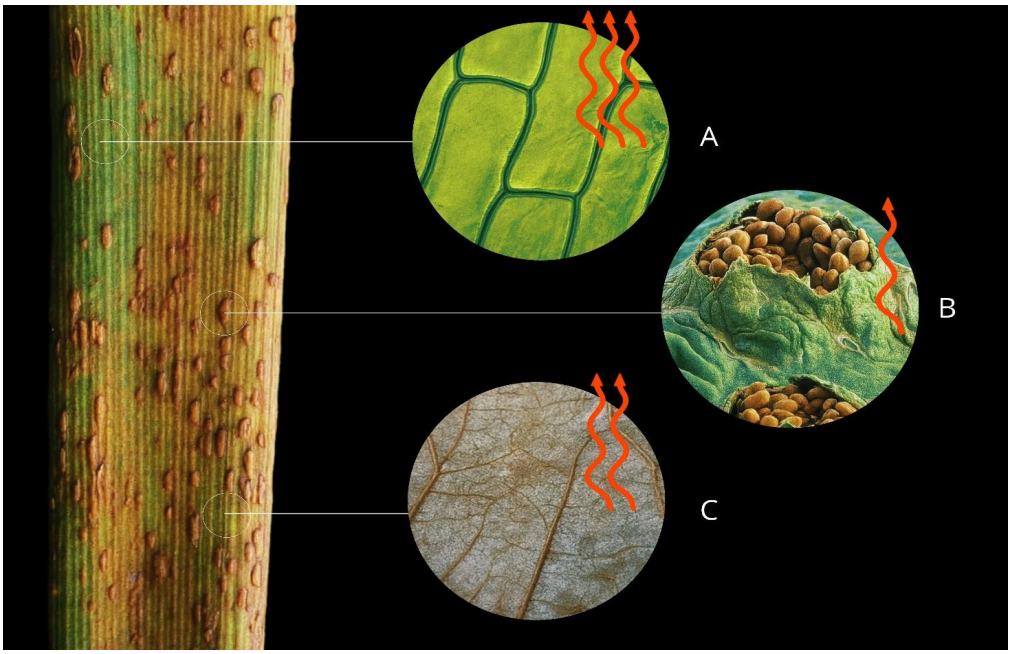

Figure 7. Wheat leaf (A - healthy areas, B - affected areas, C - dried areas)

Conclusion

The obtained data confirm that hyperspectral imaging is a highly effective tool for the detection of wheat rust and the assessment of its overall phytosanitary status. The use of hyperspectral data allowed for the analysis of differences in the spectral characteristics of lesions on the wheat ear, leaf, and stem, as well as the identification of the most significant patterns.

It has been established that healthy areas have a high level of light reflectance, which is due to normal cellular structure and its chlorophyll content. Meanwhile, the intensity in desiccated areas is noted to be at a lower level, which may be associated with moisture loss and disruptions occurring in the plant structure. It has been revealed that rust-affected zones possess low reflectances, related to tissue degradation and the accumulation of dark pigments in the pathogens, which allow them to ensure resistance to external stresses. These combined factors create a distinct spectral profile that enables reliable disease identification.

As a result, based on the analysis of spectral characteristics using the Random Forest algorithm, a classification model was built for recognising rust-affected zones, with an actual average classification accuracy of up to 94%.

Thus, this research demonstrates that the integration of hyperspectral imaging with machine learning methods enables the detection of rust and differentiation of the degree of infection by its pathogen across various plant parts, including early stages. This approach can be integrated into remote monitoring systems for wheat agroecosystems, thereby ensuring timely diagnosis of various phytopathologies.

Author Contributions

U.R.M. - concept and supervision of the work; O.A.V. - conducting the experiments; K.M.M. - discussion of the research results; F.A.A. - writing the text; Zh.S.B. - editing the text of the article.

Funding

This research is funded by the Science Committee of the Ministry of Science and Higher Education of the Republic of Kazakhstan (Grant No. AP22784689 «Development of an integrated system for remote monitoring of spring wheat agrocenoses based on spectral imaging technology for the creation of precision agriculture».

Conflict of Interest

The authors declare no conflict of interest.

Compliance with ethical standards

This article does not contain a description of studies performed by the authors involving people or using animals as objects.

References

1. Sekerova T, Tileubayeva Zh, Ydyrys A, Aitzhanova M, Bakirova K, Mutlu M, Admanova G. Assessing Kazakhstani wheat varieties by yield indicators and resistance to rust. International Journal of Biology and Chemistry. 2021;14(1):64-73. https://doi.org/10.26577/ijbch.2021.v14.i1.06
2. Genievskaya Y, Turuspekov Y, Rsaliyev A, Abugalieva S. Genome-wide association mapping for resistance to leaf, stem, and yellow rusts of common wheat under field conditions of South Kazakhstan. PeerJ. 2020. doi.org/10.7717/peerj.9820
3. Huang W, Lamb DW, Niu Z, Zhang Y, Liu L, Wang J, Wang L. Identification of yellow rust in wheat using in-situ spectral reflectance measurements and airborne hyperspectral imaging. Precision Agriculture. 2007;8:187-197. https://doi.org/10.1007/s11119-007-9038-9
4. Yao Z, Lei Y, He D. Early visual detection of wheat stripe rust using visible/near-infrared hyperspectral imaging. Sensors. 2019;19(4):952. https://doi.org/10.3390/s19040952

5. Ma H, Ye H, Huang W, Dong Y, Shi Y, Ruan C. Identification and severity determination of wheat stripe rust and wheat leaf rust based on hyperspectral data acquired using a black-paper-based measuring method. PLOS ONE. 2016;11(5):e0154648. https://doi.org/10.1371/journal.pone.0154648

6. Zhao J, Huang L, Huang W, Yuan L, Ye H. Hyperspectral measurements of severity of stripe rust on individual wheat leaves. European Journal of Plant Pathology. 2014;139:407-417. https://doi.org/10.1007/s10658-014-0397-6

7. Devadas R, Lamb DW, Backhouse D, et al. Sequential application of hyperspectral indices for delineation of stripe rust infection and nitrogen deficiency in wheat. Precision Agriculture. 2015;16:477-491. https://doi.org/10.1007/s11119-015-9390-0

8. Mutafa A, Al-Sadi A, et al. Hyperspectral signal decomposition and symptom detection of wheat rust disease at the leaf scale using pure fungal spore spectra as reference. Plant Pathology. 2021. https://doi.org/10.1111/ppa.13020

9. Terentev A, Badenko V, Shaydayuk E, Emelyanov D, Eremenko D, Klabukov D, Fedotov A, Dolzhenko V. Hyperspectral remote sensing for early detection of wheat leaf rust caused by Puccinia triticina. Agriculture. 2023;13(6):1186. https://doi.org/10.3390/agriculture13061186

10. Chossegros M, Hubbard A, Burt M, et al. Hyperspectral image analysis for classification of multiple infections in wheat. Plant Methods. 2025;21:144. https://doi.org/10.1186/s13007-025-01461-x

11. Guo A, Huang W, Ye H, Dong Y, Ma H, Ren Y, Ruan C. Identification of wheat yellow rust using spectral and texture features of hyperspectral images. Remote Sensing. 2020;12(9):1419. https://doi.org/10.3390/rs12091419

12. Wójtowicz A, Piekarczyk J, Wójtowicz M, Królewicz S, Świerczyńska I, Pieczul K, Jasiewicz J, Ceglarek J. Integrating RGB image processing and random forest algorithm to estimate stripe rust disease severity in wheat. Remote Sensing. 2025;17(17):2981. https://doi.org/10.3390/rs17172981

13. Zhang X, Han L, Dong Y, Shi Y, Huang W, Han L, González-Moreno P, Ma H, Ye H, Sobeih T. A deep learning-based approach for automated yellow rust disease detection from high-resolution hyperspectral UAV images. Remote Sensing. 2019;11(13):1554. https://doi.org/10.3390/rs11131554

14. Terentev A, Kuznetsova D, Fedotov A, Baranova O, Eremenko D. Cross-crop transferability of machine learning models for early stem rust detection in wheat and barley using hyperspectral imaging. Plants. 2025;14(21):3265. https://doi.org/10.3390/plants14213265

15. Abdulridha J, Min A, Rouse MN, Kianian S, Isler V, Yang C. Evaluation of stem rust disease in wheat fields by drone hyperspectral imaging. Sensors. 2023;23(8):4154. https://doi.org/10.3390/s23084154

16. Deng J, Wang X, Zhang J, Li H, Xue X. Quantitative estimation of wheat stripe rust disease index using unmanned aerial vehicle hyperspectral imagery and innovative vegetation indices. IEEE Transactions on Geoscience and Remote Sensing. 2023;61:4406111. https://doi.org/10.1109/TGRS.2023.3292130

17. Guo A, Huang W, Dong Y, Ye H, Ma H, Liu B, Wu W, Ren Y, Ruan C, Geng Y. Wheat yellow rust detection using UAV-based hyperspectral technology. Remote Sensing. 2021;13(1):123. https://doi.org/10.3390/rs13010123

18. Zheng Q, Huang W, Ye H, Dong Y, Shi Y, Chen S. Using continuous wavelet analysis for monitoring wheat yellow rust in different infestation stages based on unmanned aerial vehicle hyperspectral images. Applied Optics. 2020;59(24):8003-8013.

19. Atanasov AZ, Evstatiev BI, Atanasov AI, Nikolova PD. Assessment of yellow rust (Puccinia striiformis) infestations in wheat using UAV-based RGB imaging and deep learning. Applied Sciences. 2025;15(15):8512. https://doi.org/10.3390/app15158512

20. Fang S, Zhang J, Li H, Huang W. Pixel-level regression for UAV hyperspectral images: Deep learning-based quantitative inverse of wheat stripe rust disease index. Computers and Electronics in Agriculture. 2023;208:108434. https://doi.org/10.1016/j.compag.2023.108434

21. Heidarian Dehkordi R, El Jarroudi M, Kouadio L, Meersmans J, Beyer M. Monitoring wheat leaf rust and stripe rust in winter wheat using high-resolution UAV-based red-green-blue imagery. Remote Sensing. 2020;12(22):3696. https://doi.org/10.3390/rs12223696

22. Perez E, Smith L, Sun D. Wheat yellow rust monitoring by learning from multispectral UAV aerial imagery. Computers and Electronics in Agriculture. 2018;155:237-247. https://doi.org/10.1016/j.compag.2018.10.017

23. Atanasov AI, Atanasov AZ, Evstatiev BI. Application of NDVI for early detection of yellow rust (Puccinia striiformis). AgriEngineering. 2025;7(5):160. https://doi.org/10.3390/agriengineering7050160

24. Behmann J, Mahlein A-K, Rumpf T, Römer C, Plümer L. Comparison of multi- and hyperspectral imaging data of leaf rust infected wheat plants. Proceedings of SPIE. 2006. https://doi.org/10.1117/12.626531

25. Ashourloo D, Mobasheri MR, Huete A. Evaluating the effect of different wheat rust disease symptoms on vegetation indices using hyperspectral measurements. Remote Sensing. 2014;6(6):5107-5123. https://doi.org/10.3390/rs6065107

26. Li J, Zhao Y, Huang W. Inversion of plant functional traits from hyperspectral imagery enhances the distinction of wheat stripe rust severity. AI in Agriculture. 2025. https://doi.org/10.1016/j.aiia.2025.10.006

27. Polyakov IYa, Persov MP, Smirnov VA. Forecasting the development of agricultural crop pests and diseases (with practical exercises). Leningrad: Kolos; 1984. p. 318.

28. State Standard 12044-93. Methods for determination of diesease infestation. Moscow: Standartinform; 2011. p. 57.

29. Chen W, Liu L, Gao R. Reconstructing hyperspectral images from RGB images by multi-scale spectral-spatial sequence learning. Entropy. 2025;27:959. https://doi.org/10.3390/e27090959

30. Rogers M, Blanc-Talon J, Urschler M, et al. Wavelength and texture feature selection for hyperspectral imaging: A systematic literature review. Food Measure. 2023;17:6039-6064. https://doi.org/10.1007/s11694-023-02044-x

31. Xia J, Falco N, Benediktsson JA, Du P, Chanussot J. Hyperspectral image classification with rotation random forest via KPCA. IEEE Journal of Selected Topics in Applied Earth Observations and Remote Sensing. 2017;10:1601-1609. https://doi.org/10.1109/JSTARS.2016.2636877

32. Rehman SU, Qiao L, Shen T, Hua L, Li H, Ahmad Z, Chen S. Exploring the frontier of wheat rust resistance: Latest approaches, mechanisms, and novel insights. Plants. 2024;13:2502. https://doi.org/10.3390/plants13172502

33. Annan EN, Huang L. Molecular mechanisms of the co-evolution of wheat and rust pathogens. Plants. 2023;12:1809. https://doi.org/10.3390/plants12091809

34. Wang J, Chen T, Tang Y, Zhang S, Xu M, Liu M, Zhang J, Loake GJ, Jiang J. The biological roles of Puccinia striiformis f. sp. tritici effectors during infection of wheat. Biomolecules. 2023;13(6):889. https://doi.org/10.3390/biom13060889

35. Qin Y, Xia Y. Melanin in fungi: Advances in structure, biosynthesis, regulation, and metabolic engineering. Microbial Cell Factories. 2024;23(1):334. https://doi.org/10.1186/s12934-024-02614-8

36. Wang E, Dong C, Park RF, Roberts TH. Carotenoid pigments in rust fungi: Extraction, separation, quantification and characterisation. Fungal Biology Reviews. 2018;32(3):166-180. https://doi.org/10.1016/j.fbr.2018.02.002

Гиперспектралды мәліметтер бойынша бидай татының спектрлік сигнатуралары: машиналық оқыту әдістерінің әлеуеті

Р.М. Уалиева[1], А.В. Осипова[2], М.М. Каверина*[3], С.Б. Жангазин[4], Н.Н. Иқсат[5]

[1,2,3]Торайғыров университеті, Павлодар, Қазақстан

[4,5]Л.Н. Гумилев атындағы Еуразия ұлттық университеті, Астана, Қазақстан

Аңдатпа. Зерттеу гиперспектралды визуализация және машиналық оқыту әдістерін қолдана отырып, татты анықтау және зақымдануды саралау тәсілін ұсынады. Бидай масағының, жапырағының және сабағының зақымдануының спектрлік сипаттамаларындағы айырмашылықтарды талдау жарықтың шағылысуы және өсімдіктер мен қоздырғыштардың құрылымы арасындағы заңдылықтарды көрсетті. Сау аймақтарда қалыпты жасушалық

құрылымға және оның құрамындағы хлорофиллге байланысты жоғары шағылысу коэффициенті анықталды. Төмен қарқындылық ылғалдың жоғалуына және өсімдік құрылымының бұзылуына байланысты өсімдіктің құрғақ аймақтарында анықталды. Таттан зардап шеккен аймақтардың шағылысу коэффициенттерінің төмен көрсеткіштері тіндердің деградациясына және сыртқы стресстерге төзімділікке ықпал ететін қоздырғыштарда қара пигменттердің жиналуына байланысты. Бұл ауруға тән, оны нақты анықтауға мүмкіндік беретін спектрлік профильді құрайды. Нәтижесінде Puccinia graminis, Puccinia triticina қоздырғыштарының зақымдануының болуын анықтау мақсатында жалпы жіктеу дәлдігі 94% болатын таттан зардап шеккен аймақтарды тану үшін Random Forest алгоритмі негізінде жіктеу моделі құрылды. Алынған мәндер үлгінің татпен зақымданған аймақтарды анықтау қабілетінің жоғары екенін көрсетеді де, бұл бидайдың тат ауруларын инвазивті емес түрде анықтау үшін гиперспектралды деректерді ансамбльдік машиналық оқыту алгоритмдерімен біріктірілген синергетикалық талдаудың перспективасын растайды.

Түйін сөздер: гиперспектралды визуализация, спектрлік сипаттамалар, тат, бидай агроценозы, жіктеу моделі

Спектральные сигнатуры ржавчины пшеницы по гиперспектральным данным: потенциал методов машинного обучения

Р.М. Уалиева[1], А.В. Осипова[2], М.М. Каверина*[3], С.Б. Жангазин[4], Н.Н. Иксат[5]
[1,2,3]Торайгыров университет, Павлодар, Казахстан
[4,5]Евразийский национальный университет имени Л.Н. Гумилева, Астана, Казахстан

Аннотация. В исследовании представлен подход к выявлению ржавчины и дифференциации поражений с применением гиперспектральной визуализации и методов машинного обучения. Анализ различий в спектральных характеристиках поражений колоса, листа и стебля пшеницы показал закономерности между светоотражением и структурой растений и возбудителей заболеваний. Здоровые участки имеют высокий коэффициент отражения за счет нормальной клеточной структуры и содержания в ней хлорофилла. Более низкая интенсивность выявлена у засохших участков, связанных с потерей влаги и нарушением структуры растения. Пораженные ржавчиной зоны обладают низкими коэффициентами отражения, что связано с деградацией тканей и накоплением темных пигментов у возбудителей, способствующих устойчивости к внешним стрессам. Это формирует характерный спектральный профиль, позволяющий наглядно идентифицировать болезнь. В результате с целью идентификации присутствия поражений возбудителями Puccinia graminis, Puccinia triticina была построена классификационная модель на основе алгоритма Random Forest для распознавания зон, пораженных ржавчиной, с общей точностью классификации 94 %. Полученные значения указывают на высокую способность модели выявлять поражения ржавчиной, что подтверждает перспективность синергетического анализа гиперспектральных данных в сочетании с алгоритмами ансамблевого машинного обучения для неинвазивного выявления ржавчинных заболеваний пшеницы.

Ключевые слова: гиперспектральная визуализация, спектральные характеристики, ржавчина, агроценоз пшеницы, классификационная модель

Authors' information:

Ualiyeva Rimma Meyramovna – PhD, Professor, Department of Biology and Ecology, Toraighyrov University, 64 Lomov St., 140008, Pavlodar, Kazakhstan.

Osipova Anastasiya Vyacheslavovna – Master's degree student, Department of Biology and Ecology, Toraighyrov University, 64 Lomov St., 140008, Pavlodar, Kazakhstan.

Kaverina Mariya Mikhailovna – Corresponding author, Junior Researcher at the Department of Biology and Ecology, Toraighyrov University, 64 Lomov St., 140008, Pavlodar, Kazakhstan.

Zhangazin Sayan Berikovich – PhD, Associate Professor, Deputy Dean for Research of the Faculty of Natural Sciences, L.N. Gumilyov Eurasian National University, 2 Satpayev St., 010008, Astana, Kazakhstan.

Iksat Nurgul Nurkanatkyzy – PhD, Acting Associate Professor, Department of Biotechnology and Microbiology, postdoctoral researcher, L.N. Gumilyov Eurasian National University, 2 Satpayev St., 010008, Astana, Kazakhstan.

Авторлар туралы мәлімет:

Уалиева Римма Мейрамовна – PhD, профессор, «Биология және экология» кафедрасы, Торайғыров университеті КеАҚ, Ломов көшесі, 64, 140008, Павлодар, Казахстан.

Осипова Анастасия Вячеславовна – магистрант, «Биология және экология» кафедрасы, Торайғыров университеті КеАҚ, Ломов көшесі, 64, 140008, Павлодар, Казахстан.

Каверина Мария Михайловна – хат-хабар авторы, кіші ғылыми қызметкер, «Биология және экология» кафедрасы, Торайғыров университеті КеАҚ, Ломов көшесі, 64, 140008, Павлодар, Қазақстан.

Жангазин Саян Берикович – PhD, қауымдастырылған профессор, деканының ғылыми жұмыс жөніндегі орынбасары, Жаратылыстану ғылымдары факультеті, Л.Н. Гумилев атындағы Еуразия ұлттық университеті КеАҚ, Сәтбаев көшесі 2, 010008, Астана, Қазақстан.

Иқсат Нұргүл Нұрқанатқызы – PhD, доцент м.а., постдокторант,«Биотехнология және микробиология» кафедрасы, Л.Н. Гумилев атындағы Еуразия ұлттық университеті КеАҚ, Сәтбаев көшесі 2, 010008, Астана, Қазақстан.

Сведения об авторах:

Уалиева Римма Мейрамовна – PhD, профессор кафедры Биология и экология, Торайгыров университет, ул. Ломова 64, 140008, Павлодар, Казахстан.

Осипова Анастасия Вячеславовна – магистрант кафедры Биология и экология, Торайгыров университет, ул. Ломова 64, 140008, Павлодар, Казахстан.

Каверина Мария Михайловна – автор для корресподенции, младший научный сотрудник кафедры Биология и экология, Торайгыров университет, ул. Ломова 64, 140008, Павлодар, Казахстан.

Жангазин Саян Берикович – PhD, ассоциированный профессор, заместитель декана по научной работе факультета Естественных наук, Евразийский национальный университет имени Л.Н. Гумилева, ул. Сатпаева 2, 010008, Астана, Казахстан.

Иқсат Нұргүл Нұрқанатқызы – PhD, и.о. доцента кафедры Биотехнология и микробиология, постдокторант, Евразийский национальный университет имени Л.Н. Гумилева, ул. Сатпаева 2, 010008, Астана, Казахстан.